



Original Article

Development of a position sensitive CsI(Tl) crystal array

Guo-Zhu Shi ^{a, b, c}, Ruo-Fu Chen ^{a, d, *}, Kun Chen ^e, Ai-Hua Shen ^a, Xiu-Ling Zhang ^a, Jin-Da Chen ^{a, d}, Cheng-Ming Du ^a, Zheng-Guo Hu ^a, Guang-Wei Fan ^e

^a Institute of Modern Physics, Chinese Academy of Sciences, Lanzhou, 730000, China

^b School of Nuclear Science and Technology, Lanzhou University, Lanzhou, 730000, China

^c School of Nuclear Science and Technology, University of Chinese Academy of Sciences, 100049 Beijing, China

^d Fujian Institute of Innovation, Chinese Academy of Sciences, Fuzhou, 350108, China

^e School of Chemical Engineering, Anhui University of Science & Technology, Huainan, 232001, China



ARTICLE INFO

Article history:

Received 10 January 2019

Received in revised form

10 September 2019

Accepted 10 September 2019

Available online 15 September 2019

Keywords:

CsI(Tl)

Crystal array

DPC

Discretized positioning circuit

IQSP518 system

ABSTRACT

A position-sensitive CsI(Tl) crystal array coupled with the multi-anode position sensitive photomultiplier tube (PS-PMT), Hamamatsu H8500C, has been developed at the Institute of Modern Physics. An effective, fast, and economical readout circuit based on discretized positioning circuit (DPC) bridge was designed for the 64-channel multi-anode flat panel PSPMT. The horizontal and vertical position resolutions are 0.58 mm and 0.63 mm respectively for the $1.0 \times 1.0 \times 5.0 \text{ mm}^3$ CsI(Tl) array, and the horizontal and vertical position resolutions are 0.86 mm and 0.80 mm respectively for the $2.0 \times 2.0 \times 10.0 \text{ mm}^3$ CsI(Tl) array. These results show that the CsI(Tl) crystal array with low cost could be applied in the fields of medical imaging and high-resolution gamma camera.

© 2019 Korean Nuclear Society, Published by Elsevier Korea LLC. This is an open access article under the CC BY-NC-ND license (<http://creativecommons.org/licenses/by-nc-nd/4.0/>).

1. Introduction

The thallium-doped cesium iodide (CsI(Tl)) scintillator has characteristics of high density, high luminous efficiency, high radiation-hardness, low cost, etc. It is widely used in the area of nuclear physics, nuclear medicine, safety inspection, etc [1–3]. A high quality large CsI(Tl) crystal has been grown by the crystal detector research group at the Institute of Modern Physics (IMP) with Bridgman method. High purity cesium iodide was pretreated and mixed with a certain proportion TlI powder to grow CsI(Tl) crystal (the mass proportion of TlI powder is 1.5%). The optimum technical parameters and the reasonable working temperature were determined through a serial of experimental tests. The experimental results showed that the doping ratio of TlI and its distribution in the crystal were the key factors which affect the homogeneity of the crystal in response to the uniformly incident gamma rays. The CsI(Tl) crystal with uniform distribution of TlI was grown by precisely controlling the growth process. Our high performance CsI(Tl) crystal has been used in scientific and industrial

programs all over the world.

It's well known that the traditional gamma cameras are manufactured using monolithic inorganic crystals coupled with an array of photomultiplier tubes (PMTs). More recently pixelated gamma cameras with discrete detector elements coupled with readouts are developing. In the last years, new small Field of View (FOV), high-spatial resolution scintillation gamma cameras, have been applied in nuclear medicine by using the new generation of Position Sensitive Photomultiplier Tube (PS-PMT) [4]. The portable gamma cameras based on position-sensitive PMTs particularly for the nuclear medicine application, have been developed by using PS-PMT H8500 and H9500 from Hamamatsu Photonics Co., Japan. An effective, fast and economical simplified readout electronics based on DPC bridge has been employed for signal processing, which greatly reduces the development costs of nuclear medical apparatus. The spatial resolution with both pixelated scintillator array has been studied to reduce the costs for the applications of Single Photon Emission Tomography (SPECT) and Positron Emission Tomography (PET) [5–7].

In 2007, a new type of gamma camera based on a position sensitive photomultiplier tube, Hamamatsu Flat Panel H8500 coupled with CsI(Tl) scintillation crystals, was studied by C. Trotta et al. for low-energy gamma-ray detection [8]. They developed an

* Corresponding author. Institute of Modern Physics, Chinese Academy of Sciences, Lanzhou, 730000, China.

E-mail address: chenruofu@impcas.ac.cn (R.-F. Chen).

innovative technique based on CsI(Tl) scintillation crystals inserted into the square holes of a tungsten collimator. The geometrical parameters of this collimator–scintillator structure, which affect spatial resolution and sensitivity of the camera, were selected to achieve the optimal performances for clinical functional examinations. The detector sensitivity, energy resolution and spatial resolution were measured individually, and the acquired image quality was evaluated with particular attention to the pixel identification capability. This portable gamma camera was about 2 kg. It combined a miniaturized resistive chain electronic readout with a dedicated compact 4 channel ADC board. The scintillation structure was composed of 20×20 scintillator elements with $2.05 \times 2.05 \times 5.0 \text{ mm}^3$ pixels at a FOV of $49.0 \times 49.0 \text{ mm}^2$. The CsI(Tl) arrays were covered by a $100 \mu\text{m}$ thick white reflective epoxy on their five blind surfaces coupled with H8500. The experimental spatial resolution were quite consistent with the theoretical ones at different source to collimator distances.

In 2010, a CsI(Tl)/PIN detector module for high resolution SPECT and low dose photon-counting CT imaging was developed by J. Kindem et al. [9]. The cardiac SPECT system were composed of three detector heads ($20 \times 15 \text{ cm}^2$ for each) using detector modules with 6.1 mm pixels. The detector heads form a triple-head, geometry for emission scans and reconstruction to form a large transaxial FOV geometric transmission scanning using an X-ray as based source of transmission. The performance of the cardiac SPECT camera was evaluated by using anthropomorphic phantom and patient data. They developed a 2.8 mm pixel size CsI(Tl) solid state detector modules with an average energy resolution of 7.5% by improving the crystal arrays, electronics and packaging of the module. The large FOV imager showed excellent clarity and high resolution for emission bone studies and demonstrated that the reconstructed CT image quality is suitable for attenuation correction or image fusion localization.

In 2012, W. Siman and S. C. Kappadath [10] evaluated an Ergo with pixelated portable gamma camera system that consists of 11520 elements of CsI(Tl) crystals with $3 \times 3 \times 6 \text{ mm}^3$ pixels. The evaluations of Ergo gamma camera showed that it had good clinical imaging performance. This portable gamma camera has high planar sensitivity, high energy and spatial resolutions, and superior count rate performance that are comparable to other available gamma cameras. All isotope-collimator pairs demonstrated good flood-field uniformity with an integral uniformity of $\leq 5\%$ and a differential uniformity of $\leq 3\%$. The system demonstrated excellent

energy linearity with maximum discrepancy between the measured and the true value (less than 1%). The energy resolution of the $^{99\text{m}}\text{Tc}$ photo-peak was 7.4% at 140 keV.

In our work, a high-resolution gamma detector array based on a position sensitive multi-anode PS-PMT H8500C coupled with $1.0 \times 1.0 \times 5.0 \text{ mm}^3$ or $2.0 \times 2.0 \times 10.0 \text{ mm}^3$ CsI(Tl) crystal pixels was built. The CsI(Tl) crystal arrays were built by the crystal detector research group at IMP. Their one-dimensional position resolutions at both the horizontal (X) and vertical (Y) direction were measured by using the new IQSP518 data acquisition system.

2. CsI(Tl) array manufacture

The high performance CsI(Tl) crystal was grown at IMP [11]. The manufacture of the CsI(Tl) crystal array includes three steps. Firstly, the CsI(Tl) crystal block was integrally segmented into paralleled and orderly pixels by an intelligent precise dicing saw machine, so the array was not spliced from the “independent” pixels one by one. The advantage of this manufacturing process could ensure the parallelism among pixels, at least. Secondly, a mixture of TiO_2 powder and optical epoxy resin glue, as a light reflective material, is irrigated into the intervals among the pixels under vacuum condition. Thirdly, the surface of light readout end of the CsI(Tl) array is optically polished. The hardness, color and light reflection efficiency of the mixture depends very sensitively on the ratio of TiO_2 powder and the light epoxy resin glue. The mass ratio of TiO_2 powder and epoxy resin glue is about 1:10 used in the experiment.

There are two sizes of the CsI(Tl) array. One of the produced CsI(Tl) array consists of 24×23 scintillator elements with $1.0 \times 1.0 \times 5.0 \text{ mm}^3$ pixels, and the whole cross section including the outer light reflective material is $30.4 \times 31.9 \text{ mm}^2$. The thickness of light reflective material (dead zone) between the pixels is 0.1 mm, measured by optical microscopy of Olympus Corporation. The other CsI(Tl) array consists of 22×22 scintillator elements with $2.0 \times 2.0 \times 10.0 \text{ mm}^3$ pixels, and the whole cross section including the light reflective material is $49.9 \times 51.2 \text{ mm}^2$. The thickness of light reflective material (dead zone) between the pixels is 0.3 mm.

To eliminate the possibly occurred bubbles during the mixing procedure of the TiO_2 powder and the optical epoxy resin glue, a vacuum system has been employed and the maximum vacuum degree was about 0.1 Pa. The schematic diagram of the vacuum system is shown in Fig. 1. And the position sensitive CsI(Tl) arrays are shown in Fig. 2.

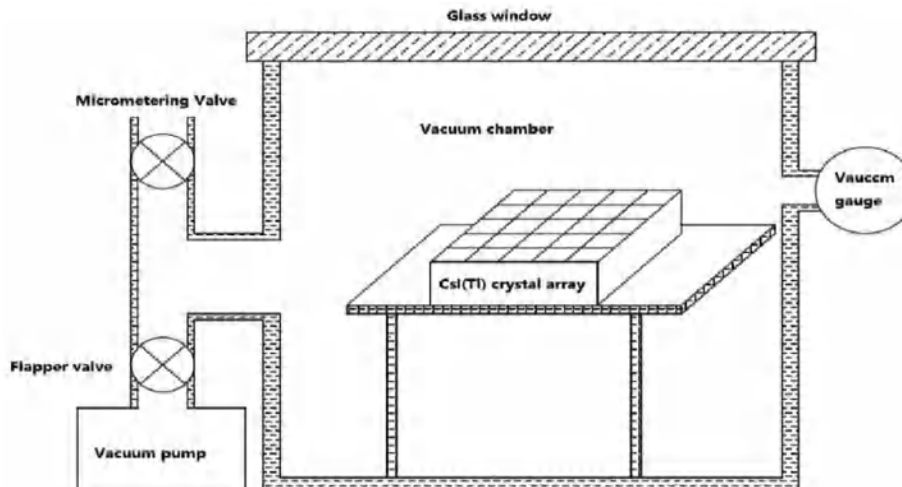


Fig. 1. The schematic drawing of perfusion and exhaust for the CsI(Tl) crystal array.

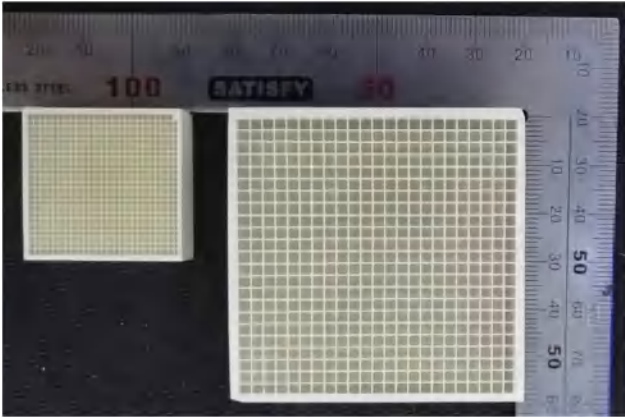


Fig. 2. Pictures of the CsI(Tl) crystal array (Cross sectional image of the CsI(Tl) crystal array with pixels of 1.0 × 1.0 mm² (left) and 2.0 × 2.0 mm² (right)).

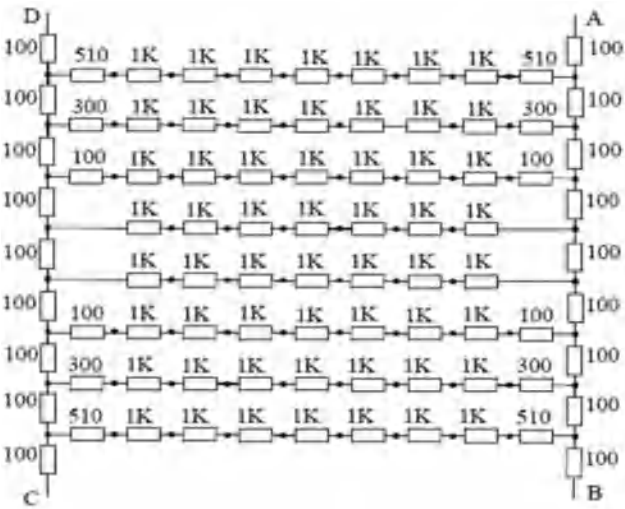


Fig. 3. The resistor network of DPC readout circuit.

3. Experiments

3.1. Readout circuit of the PSPMT

Usually the position-sensitive PMT, H8500C, together with high-resolution modular imaging detector, is used to achieve compact size and fine performances [12]. It has 64 discrete anodes with 8 × 8 arrays, and the module size of the pipe is 52 × 52 × 28 mm³, the effective area of the photocathode is 49 × 49 mm². The research of the high-resolution imaging detector module coupled with this PMT has become a hot topic.

The readout circuit must be very complex on one-by-one anode readout mode, so a simplified circuit for position readout methods based on DPC has been developed [13–15]. Each anode signal of the 64-channel multi-anode PMT corresponds to node of the middle 8 resistance strings, and the resistance values for each resistor are shown in Fig. 3, the units are in Ohm (Ω). The entire resistance network relies on 86 resistors with different resistance values for signal processing, where R_{AD} = R_{BC} = 1.518 kΩ, R_{DC} = R_{AB} = 0.849 kΩ. The 4-channel readout signals of A, B, C and D from the DPC bridge resistance network should give the X, Y positions of the incident gamma rays in the CsI(Tl) crystal array with the following formula (1) [16].

$$X = \frac{(V_A + V_B) - (V_C + V_D)}{V_A + V_B + V_C + V_D}, Y = \frac{(V_A + V_D) - (V_C + V_B)}{V_A + V_B + V_C + V_D} \quad (1)$$

3.2. Experimental system based on IQSP518 data acquisition

The experimental diagram for the present measurement is shown in Fig. 4. The position sensitive PMTs, H8500C, were coupled with two different sizes of CsI(Tl) arrays (1.0 × 1.0 mm² and 2.0 × 2.0 mm² pixel) individually. The ²²Na radioactive source was used. The positive electrons emitted from ²²Na β⁺ decay source will annihilate in the CsI(Tl) crystal, which results in a production of two γ-rays of 511 keV in opposite directions. These two γ-rays can be used to determine the Line of Response (Line of Response, LOR). The distance between the ²²Na source and the CsI(Tl) array is about 15 cm. The tests were carried out using the DAQ platform of IQSP518 (Vertilon company, USA) which is an expandable multi-parallel system based on digital signal processor (DSP) with high-precision and high-speed. The system has the advantages of 8-channel charge integration and well compatibility with PMT, APD, SiPM and other multi-channel detectors. A real-time label was added in the data event records by using a variety of trigger modes. In order to keep the synchronization in the test platform, a specially designed data acquisition board SIB064-1018 from the Vertilon company was used in the platform. The PMT's 64 anodes outputs can be simplified to the 4-channel position signal by DPC bridge circuit designed by ourselves, and the outputs of the dynode signal turn into a variety of trigger signals. The bridge circuit not only simplifies the subsequent electronic system but also reduces the costs. Two-dimensional images of a flood field irradiation and their cross-section spectra of the crystal array were thus obtained by the charge-division processing method.

4. Experimental results

The crystal arrays were coupled with the H8500C by silicone grease to improve the collection efficiency of scintillating light. Two-dimensional images of a flood field irradiation and their cross-section spectra are shown in Fig. 5–8, respectively. In the

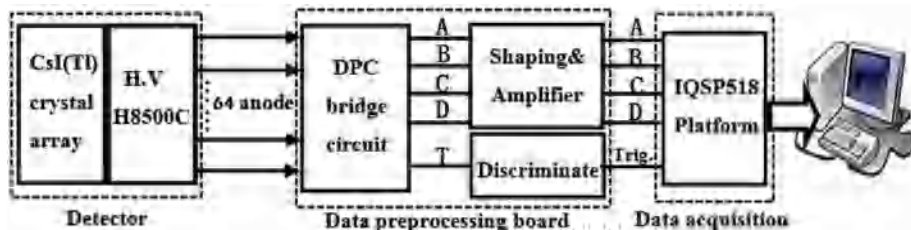


Fig. 4. The experimental diagram for the test.

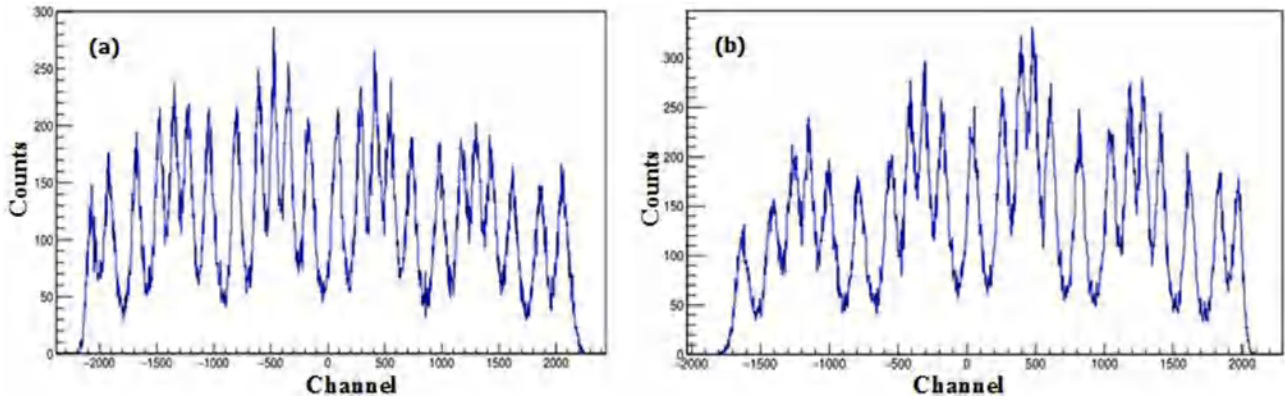


Fig. 5. Horizontal (a) and vertical (b) slices of a flood field irradiation image with $1.0 \times 1.0 \text{ mm}^2$ pixel array.

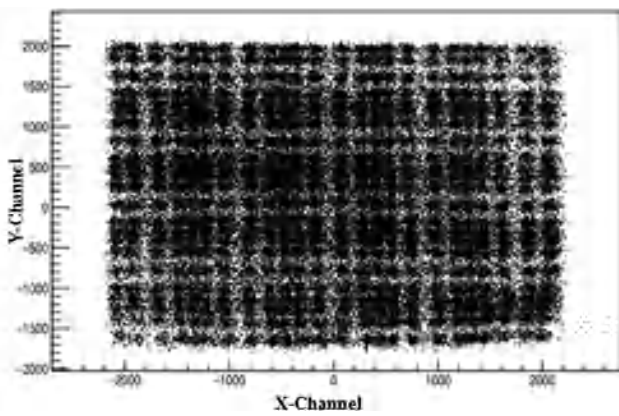


Fig. 6. Two-dimensional images of a flood field irradiation with $1.0 \times 1.0 \text{ mm}^2$ pixel array.

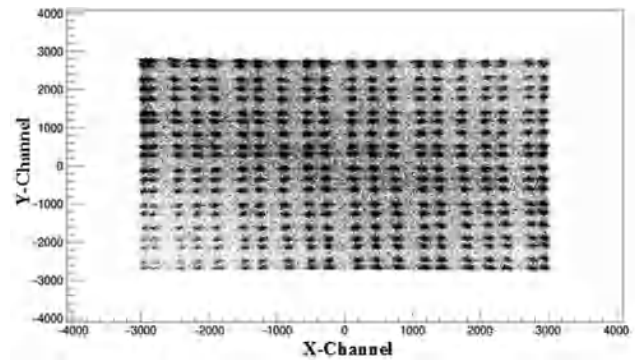


Fig. 8. Two-dimensional images of a flood field irradiation with $2.0 \times 2.0 \text{ mm}^2$ pixel array.

positioning histogram all the CsI(Tl) crystal elements in the block were clearly separated. The peak profiles of the image along different vertical lines are also shown in Figs. 5 and 7. A good valley to peak ratio is obtained.

The projections of all pixels in two different sizes CsI(Tl) crystal arrays on the horizontal and vertical directions are shown in Figs. 5 and 7. However, two pixels were disappeared in the horizontal and vertical projection for 22×22 crystal elements with $2.0 \times 2.0 \text{ mm}^2$ pixel array in Fig. 7. It's reasonably speculated that the edge information points were slightly distorted and even lost due to cross-

talk and edge effect of multi-anode PMT. The peaks with better resolution at the center will be chosen for the Gaussian fitting rather than the peaks at the edge. In current work, only 23 ($1.0 \times 1.0 \text{ mm}^2$ pixel) and 17 peaks ($2.0 \times 2.0 \text{ mm}^2$ pixel) in flood field irradiation image were selected respectively for calculating their one-dimensional position resolutions by the Gaussian fitting. The $\bar{\sigma}$ and d (variables are defined below) values were obtained by fitting the cross-section of a flood field irradiation image in the horizontal and vertical directions using formula (1), and the results were shown in Table 1. However, because of the poor energy resolution of CsI(Tl) crystal array and the lack of energy normalization of crystal elements, the energy resolution of the whole detector is

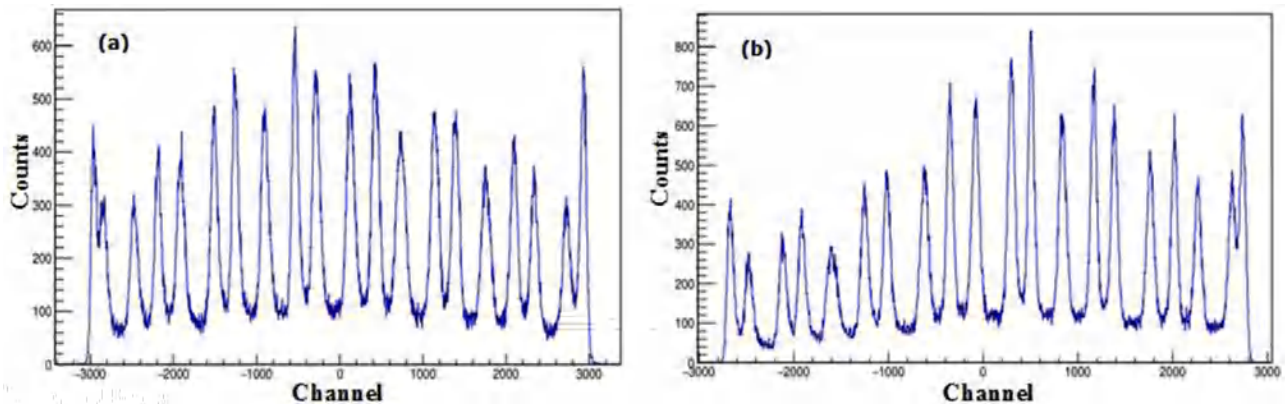


Fig. 7. Horizontal (a) and vertical (b) slices of a flood field irradiation image with $2.0 \times 2.0 \text{ mm}^2$ pixel array.

Table 1
Parameters list of the cross-section of a flood field irradiation image for crystal arrays.

Pixel size	Position parameters			
	Fitting and measuring parameters	Horizontal (X)	Vertical (Y)	Notes
24 × 23 crystal array with 1.0 × 1.0 mm ² pixel	$\bar{\sigma}$	46.2	44.0	① the 0.1 mm thickness of the inter-scintillator.
	$d(\text{channel})$	3975.0	3594.3	② the number of effective Gaussian fitting peaks is 23.
	$L(\text{mm})$	21.4	21.8	
22 × 22 crystal array with 2.0 × 2.0 mm ² pixel	$\bar{\sigma}$	52.9	44.6	① the 0.3 mm thickness of the inter-scintillator.
	$d(\text{channel})$	5200.8	4738.4	② the number of effective Gaussian fitting peaks is 17.
	$L(\text{mm})$	36.1	35.9	

not given here.

In this paper, we define the position resolution as the average of the one-dimensional position resolution of all crystal pixel bars. The formula for calculating FWHM values of one-dimensional position resolution is:

$$\text{FWHM} = \frac{L}{d} \times \bar{\sigma} \times 2.36 \quad (2)$$

where L denotes the distance between the two outermost pixel centers for the all selected Gaussian fitting peaks in the horizontal and vertical directions, d denotes the difference between the first fitting peak channels and the last fitting peak channels, $\bar{\sigma}$ denotes the average values of sigma for all Gaussian fitted peaks.

The cross section and the dead zone size of the crystal pixel bars can be given by optical microscopy. The observed values of $\bar{\sigma}$ and d are shown in Table 1, the FWHM of one-dimensional position resolution can be calculated. For the CsI(Tl) crystal array of 24 × 23 elements with 1.0 × 1.0 mm² pixel cross section, the horizontal and vertical position resolution were 0.58 mm and 0.63 mm respectively. For the CsI(Tl) crystal array of 22 × 22 elements with 2.0 × 2.0 mm² pixel cross section, the horizontal and vertical position resolution were 0.86 mm and 0.80 mm respectively. There is no essential difference between horizontal (X) and vertical (Y) direction for the one-dimensional position resolution values. The difference in the position resolution values of the two directions is only due to the light yield uniformity of each pixel in a CsI(Tl) crystal array is not absolutely consistent, including the crystal elements size, electronics, the matching of resistance and capacitance in the DPC board, and so on. These factors will lead to uncertainty of measurement results of the position resolution in between difference directions, it would require more developments in hardware and software to obtain a uniform image, including replacement readout circuit and improvement the uniformity of optical properties of CsI(Tl) crystal pixels.

It is worth mentioning that the cross section of CsI(Tl) array with 2.0 × 2.0 × 10.0 mm³ pixel size is 49.9 × 51.2 mm², while the active photo cathode area of H8500C is only 49.0 × 49.0 mm² and is covered by an 8 × 8 anode array. Thus, the signals from the marginal pixels are lost. Of course, the loss of marginal pixels signals is also affected by crosstalk and edge effect of multi-anode PMT. As shown in Figs. 6 and 8, it is evident that the measured pixel positions are not equally spaced from two-dimensional images of a flood field irradiation, we took the mismatch of the characteristics of the capacitance and resistance in the DPC board as the main reason. The structure of simplified readout circuit based on DPC is easy to be realized, and it makes the signal acquisition and processing of the back-end much easier and thus reduce the cost of the whole system. However, when it is used for the readout of the high-resolution imaging detector, the nonlinear localization and compression effect in the region near the edge of the detector will become obvious, which will affect the positioning resolution and

image FOV of the detector. We are going to replace DPC by other readout circuits, such as symmetric resistive charge division circuit (Charge-SCD) [17] for better resolution. Furthermore, the optimization of the optical coupling between the scintillation crystal array and the H8500C entrance window with optical grade silicone grease must be done so as to improve the location accuracy and increase the image FOV, and then effectively increase the useable area of the detector in the future.

5. Conclusion

Our experiments reveal that the position resolution of the CsI(Tl) crystal array depends on the pixel size. Good position resolution and flood field irradiation image could be obtained by using the crystal array with small pixel size, and as a result, they can meet imaging device requirement for high-resolution, large FOV, good spatial linearity. The DPC processing circuit can simplify the integration of subsequent electronics system, which is of great importance for reducing the cost and miniaturize the imaging detectors and gamma camera design using the multi-anode photomultiplier in medical imaging. Our work will provide technological support for the feasibility of the industrialization of portable gamma cameras in the future. More detail and improvement study will be carried out in the near future.

Acknowledgments

This work was supported by the National Key Research and Development Program of China (2016YFB0701001), General Program of National Natural Science Foundation of China (11475234), Joint Fund for Research Based on Large-Scale Scientific Facilities (U1532131) and the Function Development Project of Chinese Academy of Sciences (2020G111).

Appendix A. Supplementary data

Supplementary data to this article can be found online at <https://doi.org/10.1016/j.net.2019.09.003>.

References

- [1] Bo Kyung Cha, Jeong-Hyun Shin, Jun Hyung Bae, et al., Scintillation characteristics and imaging performance of CsI:Tl thin films for X-ray imaging applications, Nucl. Instrum. Methods Phys. Res. 604 (2009) 224–228. <https://doi.org/10.1016/j.nima.2009.01.177>.
- [2] E. Seeram, Digital mammography: an overview, Can. J. Med. Radiat. Technol. 36 (2006) 15–23. [https://doi.org/10.1016/S0820-5930\(09\)60082-7](https://doi.org/10.1016/S0820-5930(09)60082-7).
- [3] M.T. Gerieke, C. Blessingeret, et al., A current mode detector array for γ -ray asymmetry measurements, Nucl. Instr. and Meth A 540 (2005) 328–347. <https://doi.org/10.1016/j.nima.2004.11.043>.
- [4] Hamamatsu technical data sheet H8500-H8500B, H9500, printed in Japan, <http://www.hamamatsu.com>, February 2005.
- [5] R. Pani, et al., Imaging detector designs based on flat panel PMT, Nucl. Instrum. Methods A 527 (2004) 54–57. <https://doi.org/10.1016/j.nima.2004.03.037>.
- [6] M. Giménez, J. M Benlloch, et al., Medium field of view multiflat panel-based

- portable gamma camera, *Nucl. Instrum. Methods A* 525 (2004) 298–302. <https://doi.org/10.1016/j.nima.2004.03.077>.
- [7] D. Herbert, N. Belcari, et al., A comparison of the imaging performance of different PSPMTs for PET applications, *Nucl. Instrum. Methods A* 518 (2004) 399–400. <https://doi.org/10.1016/j.nima.2003.11.033>.
- [8] C. Trotta, R. Massari, N. Palermo, et al., New high spatial resolution portable camera in medical imaging, *Nucl. Instrum. Methods A* 577 (2007) 604–610. <https://doi.org/10.1016/j.nima.2007.03.037>.
- [9] J. Kindem, C. Bai, R. Conwell, CsI(Tl)/PIN solid state detector for combined high resolution SPECT and CT imaging, *Proc. IEEE Nucl. Sci. Symp.* (2010) 1987–1990. <https://doi.org/10.1109/NSSMIC.2010.5874123>.
- [10] W. Siman, S.C. Kappadath, Performance characteristics of a new pixelated portable gamma camera, *Med. Phys.* 39 (2012) 3435–3444. <https://doi.org/10.1118/1.4718874>.
- [11] Ruo-Fu Chen, X.U. Hu-Shan, et al., Property measurement of the CsI(Tl) crystal prepared at IMP, *Chin. Phys. C* 32 (2008) 135–138.
- [12] Qi Hui Rong, Jin chuan Wang, Guo qing Xiao, et al., Investigation of predigested processing 64 signals of flat-panel PMT, *Nucl. Electron. Detect. Technol.* 26 (2006) 450–453 (in Chinese).
- [13] S. Siegel, R.W. Silverman, Shao YiPing, et al., Simple charge division readouts for imaging scintillator arrays using a multi-channel PMT, *IEEE Trans. Nucl. Sci.* 43 (1996) 1634–1641. <https://doi.org/10.1109/23.507162>.
- [14] David Stratos, Georgiou Maria, et al., Comparison of three resistor network division circuits for the readout of 4×4 pixel SiPM arrays, *Nucl. Instrum. Methods Phys. Res.* 702 (2013) 121–125. <https://doi.org/10.1016/j.nima.2012.08.006>.
- [15] S. Vecchio, M. Camarda, et al., Preliminary study of different readout strategies for a positron emission mammograph head, *Nucl. Instrum. Methods Phys. Res.* 569 (2006) 264–268. <https://doi.org/10.1016/j.nima.2006.08.025>.
- [16] C.J. Borkowski, M.K. Kopp, Some applications and properties of one- and two-dimensional position sensitive proportional counter, *IEEE Trans. Nucl. Sci.* 17 (1970) 340–349. <https://doi.org/10.1109/TNS.1970.4325710>.
- [17] V. Popov, et al., *IEEE Nuclear Science Symposium Conference Record* (2003) 2156.